Simulation of a Multiple Substrate Reactor for Chemical Vapor Infiltration of Pyrolytic Carbon Within Carbon-Carbon Composites

P. McAllister and E. E. Wolf
Dept. of Chemical Engineering, The University of Notre Dame, Notre Dame, IN 46556

A model for a pilot-scale chemical vapor infiltration (CVI) reactor in which multiple substrates are densified simultaneously by carbon deposition from a pyrolyzing hydrocarbon is presented. Kinetic expressions and parameters and transport properties for carbon deposition from propylene determined from experimental studies and a single substrate CVI model are incorporated into the pilot reactor model. The two-dimensional transport equations for heat, mass and momentum transfer are solved for the entire reactor to simulate the effects of varied operating conditions on substrate densification throughout the reactor during the CVI process. Of the conditions simulated, the reactor temperature was found to have the most significant impact on both the uniformity of densification and the process time required. As the temperature increased, the uniformity of densification decreased and the time at which pore blockage at the outer surface occurred was shortened. Increasing the hydrocarbon feed concentration shortened the process time, but did not affect the final level of densification, while the feed rate only affected CVI at intermediate times. Comparison between experimental pilot reactor results and model predictions were satisfactory at short and long times, but agreement was less satisfactory at intermediate times.

Introduction

The chemical vapor infiltration (CVI) process is used in the fabrication of composite materials to densify porous preforms by deposition of a solid product from a reacting gas phase. Several recent publications (Gupte and Tsamopoulos, 1989, 1990; Tai and Chou, 1989; Middleman, 1989; Jensen and Melkote, 1989; Chung et al., 1991; Chung and McCoy, 1991; McAllister and Wolf, 1991) have presented models for the densification of a single substrate CVI process; however, in industrial practice multiple substrates are densified simultaneously in much larger CVI reactors. In the case of carbon-carbon disc brakes, pilot-scale reactors are loaded with a single stack of carbon fiber substrates, while production furnaces may contain multiple stacks of substrates. In many CVI reactors, significant gradients in substrate densification can occur not only within substrates, but also along the length of the reactor due to depletion of the hydrocarbon from the gas phase, temperature gradients within the reactor, or the prevailing flow patterns. The additional surface area and the obstructions to flow due to the multiple substrates significantly increase the complexity of pilot or full-scale CVI reactor models. In addition to the consideration of the coupled phenomena of diffusion, reaction, and deposition within each substrate treated previously (McAllister and Wolf, 1991), the transport of heat, momentum and mass in the unoccupied regions of the reactor must be modeled to represent the multisubstrate reactor realistically. Thus, a CVI reactor model must account for nonisothermalities, bulk flow of carrier gas and reactants outside the substrates, diffusional transport of reactants within substrates, homogeneous reactions both in the bulk stream and within the porous substrates, heterogeneous deposition of carbon and the time-dependent pore structure of each substrate in the reactor.

While models including diffusion/reaction with solid product formation have been applied to CVI processes (Gupte and Tsamopoulos, 1989, 1990; Tai and Chou, 1989; Middleman,

Correspondence concerning this article should be addressed to E. E. Wolf.

1989; Jensen and Melkote, 1989; Chung et al., 1991; Chung and McCoy, 1991; McAllister and Wolf, 1991), they have been limited to a single pore (Gupte and Tsamopoulos, 1989), a single substrate (Gupte and Tsamopoulos, 1990; Tai and Chou, 1989; Jensen and Melkote, 1989; Chung et al., 1991; Chung and McCoy, 1991), or a single substrate diffusion-reaction model linked to a well-mixed reactor model (Middleman, 1989) or a plug-flow reactor (McAllister and Wolf, 1991). While no literature reports of models for multiple substrate CVI reactors have been found, many similarities exist between hot wall CVI reactors and hot wall reactors used for low pressure chemical vapor deposition (LPCVD) of electronic thin films such as polycrystalline Si, SiO_2, and Si_3N_4 (Jensen, 1984). In hot-wall LPCVD reactors, for which models have been presented, the reactant gas(es) enter the reactor and flow around a stack of flat wafers placed in a holder and heterogeneous and/or gas phase reactions lead to deposition of a thin coating on the nonporous wafer substrates. The primary difference between CVI and LPCVD processes is diffusion, reaction and deposition within the void structure of porous substrates which occurs in CVI, rather than deposition on a flat surface as in LPCVD. In addition, pressures less than one torr are used in LPCVD which impacts the relative importance of convection and diffusion contributions to heat and mass transport.

Because of the physical similarities of the reactor configurations used for LPCVD and CVI, it is relevant to cite the LPCVD modeling literature. Kuiper et al. (1982) presented a highly simplified LPCVD reactor model which indicated that significant variations in the LPCVD film growth rate could occur along the length of the reactor. Jensen and Graves (1983) presented a more extensive analysis which included effects of changes in moles due to reaction, imposed temperature profiles, an inert diluent and recycling of reactor effluent. Jensen and Graves (1983) fit this model to experimental results for LPCVD of silicon from SiH_4 and found fair agreement between experimental data and model predictions. These authors also found that certain imposed wall temperature profiles and feed recycle could improve the uniformity of film growth throughout the reactor. Roenigk and Jensen (1985) developed a general model incorporating multicomponent transport effects and reaction kinetics representing both gas phase and surface reactions. The simulated LPCVD results reported by these authors for deposition of pure polycrystalline Si compared favorably with experimental results. Also, Roenigk and Jensen (1985) modeled a hypothetical, continuous, moving wafer LPCVD reactor and found that a continuous process could be advantageous in terms of process automation and film uniformity from wafer to wafer.

Middleman and Yeckel (1986) examined the effects of diffusion and convection on the rate and uniformity of deposition in LPCVD reactors and found that the assumption of minor effects of convection between wafers made by previous authors was justified, and the assumption of plug flow instead of laminar flow in the annular region had little effect on model predictions. In more recent work, Yeckel and Middleman (1989) presented a model for an entire isothermal LPCVD reactor which included homogeneous reactions but instead of solving the momentum transport equation, plug flow was assumed in the annular region and convection was neglected in the interwafer spaces. Also, simulations by Yeckel and Middleman (1990) indicated improved uniformity of film growth in reactors with modified wafer holders and interwafer screens. Houtman et al. (1985) illustrated the application of finite element methods for the simultaneous solution of the momentum, heat and mass-transfer equations with case studies of horizontal and vertical CVD reactors which have become possible with increased computational power and more efficient numerical methods. The modeling approach suggested by Houtman et al. (1985), in which the complete transport equations were solved for the entire reactor was followed in this article.

The experimental studies and kinetic modeling studies of carbon deposition during propylene pyrolysis presented by McAllister et al. (1990), and the diffusion, reaction and deposition model for CVI of porous carbon fiber substrates presented by McAllister and Wolf (1991) have provided the foundation for the development of a realistic multisubstrate CVI reactor model. Thus, the primary objective of this work was to develop a model for a multiple substrate CVI reactor loaded with a stack of porous substrates in order to predict the densification of each substrate with respect to time for various operating conditions. The diffusion, reaction and deposition modeling concepts employed previously (McAllister and Wolf, 1991) were incorporated into the model to account for the infiltration of carbon within the porous materials. Also, the kinetic expressions and parameters, and transport properties reported in prior publications (McAllister and Wolf, 1991; McAllister et al., 1990) for CVI of carbon during propylene pyrolysis were used in the model to represent a real and well characterized CVI system. The effects of variations in the adjustable operating conditions (temperature, flow rate, propylene concentration, and spacing between substrates) have been examined and the implications are discussed. Finally, model predictions were compared with experimental data for densification of carbon filler/resin char matrix substrates in a multisubstrate CVI reactor.

CVI Reactor Model

CVI reactor description

A schematic of a pilot-scale CVI reactor configuration similar to the types used in the industrial fabrication of carbon-carbon disc brakes is shown in Figure 1. Because of the axisymmetric geometry, the reactor model developed here considers two-dimensional transport for the axial cross section shown in Figure 1. The reactor is positioned vertically, with the gas inlet at the bottom and the outlet at the top. The reactor length is $L_{r\times r}$, with $z=0$ located at the inlet at the bottom of the reactor, and $z=L_{r\times r}$ at the outlet. After entering the reactor, gases flow upward through a preheat zone of length L_{pre}, and then enter the load zone in which the porous substrates are placed. In the load zone of the reactor, carbon composite substrates are stacked one atop the other with small spacers placed between each substrate to allow access of the gas phase to the substrate surfaces. In this model, the substrates are considered to be cylindrical rings with an inner radius of R_i, an outer radius of R_o, and a thickness of L_{dsc} as shown in the expanded view on the left of Figure 1. Although cylindrical, the discs appear as rectangular obstructions in the axial cross section, and the space between substrates is equal to L_{spc}. The discs are stacked to as near the outlet of the reactor as possible with the number of substrates per load depending on the reactor

length, disc thickness, separation between discs, and length of the preheat zone.

The reactor has a hot external wall and will be considered to have a temperature profile imposed at the inner wall of the graphite susceptor. Heat is supplied to the outer wall of the reactor, and its temperature is controlled from thermocouples readings at several locations between the outer reactor wall and the susceptor. In this manner, a temperature profile is imposed at the reactor wall. The pressure at the outlet of the reactor is fixed at atmospheric and due to the low flow rates commonly used, the pressure drop across the reactor is small. The feed to the reactor is a hydrocarbon gas diluted in an inert carrier gas such as He or N_2 and fed at a volumetric flow rate of Q, a temperature of T_{in} and hydrocarbon mole fraction of y_{in}. The feed gases are brought to reaction temperature in the preheat zone of the furnace and as the gas is heated, thermal pyrolysis of the hydrocarbon produces a carbon precursor which deposits on surfaces present in the reactor including the substrates and the reactor walls. The processes which occur throughout the reactor include chemical reaction, mass transport, momentum transport, heat transport, and pore structure changes in the substrates due to deposition. The relative contributions on convection and diffusion in the transport equations will vary with position in the reactor with diffusion being dominant inside the porous substrates, possible contributions of both convection and diffusion in the space between discs and primarily convective transport in the regions of unobstructed flow.

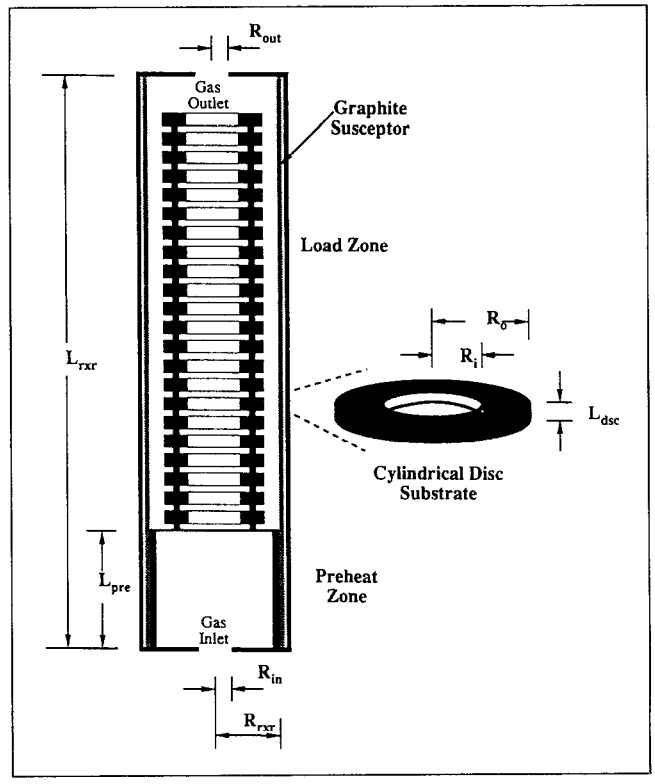

Figure 1. Schematic diagram of a multisubstrate pilot CVI reactor.

CVI reactor model development

The CVI reactor described in the previous section involves simultaneous transport and physico-chemical phenomena which must be modeled to simulate the behavior of such a reactor. The approach of this work was to develop a model for the reactor configuration in Figure 1 by coupling the kinetic studies reported in previous work (McAllister et al., 1990) and modeling investigations of diffusion, reaction and carbon deposition for a single substrate (McAllister and Wolf, 1991) with the appropriate equations for transport of mass, heat and momentum in the multisubstrate pilot CVI reactor. To effectively model the pilot-scale CVI reactor, the equations for momentum, heat, and mass transfer must be solved with the appropriate parameters and source terms to obtain the flow field, temperature field, concentration fields, and amount of carbon deposited within each substrate. Thus, the conservation equations for the CVI reactor model are:

Equation of Continuity:

$$\frac{\partial \rho}{\partial t} + \nabla \cdot \rho v = 0 \tag{1}$$

Transport of Momentum:

$$\frac{\partial \rho}{\partial t} + \nabla \cdot (\rho v v - \mu \nabla v) = -\nabla P - \nabla \cdot (\tau + \mu \nabla v) + \rho g \tag{2}$$

Transport of Energy:

$$\frac{\partial \rho C_p T}{\partial t} + \nabla \cdot (\rho v C_p T - k \nabla C_p T) = S_r \tag{3}$$

Transport of Mass:

$$\frac{\partial \rho \omega_i}{\partial t} + \nabla \cdot (\rho v \omega_i - \rho D_{\text{effi}} \nabla \omega_i) = r_i \tag{4}$$

Where, ρ is the fluid density, v is the velocity vector, t is the time, μ is the fluid viscosity, P is the pressure, τ is the stress tensor, g is the gravitational force vector, C_p is the constant pressure specific heat, T is the temperature, k is the thermal conductivity of the medium, ω_i is the mass fraction of species i, D_{effi} is the effective mass diffusivity of species i, and r_i is the net rate of generation of species i. In the energy equation, S_r is the rate of heat generation which was set equal to zero, and the terms corresponding to viscous dissipation and compression have been neglected due to the minor contributions to heat transfer under CVI conditions. Note that Eqs. 2-4 are arranged so that the lefthand side contains a transient term, and convection and diffusion terms while the right side consists of source terms. The equations are written in this standard form to facilitate solution by the numerical solver which is discussed below. For the CVI reactor described earlier, these general equations are formulated in cylindrical coordinates for a two-dimensional (r-z), nonisothermal and nonsteady-state system. Before discussing the solution of these equations, some

Table 1. Summary of Primary Reactions Involved in Carbon Deposition During Propylene Pyrolysis

Conversion of Propylene

$$C_3H_6 \xrightarrow{k_1} \text{pyrolysis products}$$

Initiation of Carbon Precursor

$$C_3H_6 \xrightarrow{k_i} I\cdot$$

Nucleation and Growth of Precursor

$$I\cdot + M \xrightarrow{k_p} IM\cdot$$

$$R_n\cdot + M \xrightarrow{k_p} R_{n+1}\cdot + M \xrightarrow{k_p} R_c\cdot$$

Deposition of Carbon

$$R_c\bullet + S \xrightarrow{k_p} R_cS$$

Table 2. Summary of Random Pore Model and Effective Diffusivity Equations

Dimensionless Pore Radius

$$\xi = r_p/r_{po}$$

Porosity Relation

$$\frac{\theta}{\theta_0} = \xi^2\left(\frac{G-\xi}{G-1}\right)$$

Surface Area Relation

$$\frac{a}{a_o} = \xi\left\{\frac{\frac{2}{3}G-\xi}{\frac{2}{3}G-1}\right\}$$

Relation Between Pore Radius, Porosity, and Surface Area

$$\frac{\partial\theta}{\partial\xi} = r_{po}\,a$$

Geometric Parameter, G

$$G^3 - \frac{27}{4\theta_o}G + \frac{27}{4\theta_o} = 0$$

Effective Diffusivity

$$D_{eff} = D_{eff_o}\left(\frac{\theta}{\theta_o}\right)^2$$

additional information is required to realistically represent the physics and chemistry of a carbon CVI reactor.

According to the reaction scheme reported previously (McAllister et al., 1990), and summarized in Table 1, the gas phase concentrations of propylene and the carbon precursor must be determined to successfully predict carbon deposition. Thus, the kinetic expressions derived elsewhere (McAllister and Wolf, 1991) for the net rate of generation of propylene and the carbon precursor in terms of mass fractions are given by Eqs. 5 and 6.

$$r_1 = -k_1'\omega_1^{1.45} \tag{5}$$

$$r_2 = k_i'\omega_1 - a_n k_d'\omega_2 \tag{6}$$

One additional equation must be solved simultaneously with the above equations to represent the changing pore structure of each substrate. Thus, the rate of change of the average pore radius is written in terms of the precursor mass fraction in Eq. 7.

$$\frac{\partial\rho\xi}{\partial t} = -k_r'\omega_2 \tag{7}$$

Where ξ is the dimensionless pore radius normalized by its initial value, and the above rate constants are defined as:

$$k_1' = \frac{\rho^{1.45}}{M_1^{0.45}}k_{1o}\exp\left(\frac{-E_1}{RT}\right) \tag{8}$$

$$k_i' = \frac{\rho}{M_1}k_{io}M_2\exp\left(\frac{-E_i}{RT}\right) \tag{9}$$

$$k_d' = a_o\rho\,k_{do}\exp\left(\frac{-E_d}{RT}\right) \tag{10}$$

$$k_r' = \frac{\rho^2}{r_{po}\rho_c}k_{do}\exp\left(\frac{-E_d}{RT}\right) \tag{11}$$

M_1 and M_2 are the molecular weights of propylene and the carbon precursor, respectively, a_o is the surface area per unit substrate volume, r_{po} is the average pore radius, ρ_c is the density of the deposited carbon. The preexponential factors (k_{1o}, $k_{io}M_2$ and k_{do}) and activation energies (E_1, E_i and E_d) were determined by a combination of experimental investigations (McAllister et al., 1990) and laboratory reactor modeling (McAllister and Wolf, 1991). The random pore model of Petersen (1957) which relates the substrate porosity and surface area to the average pore radius is also used in the model. The effective diffusivity is related to the molecular diffusivity and the porosity of the substrate according to the expressions of Satterfield (1980) and Guzman and Wolf (1979). The relevant pore model and effective diffusivity equations are listed in Table 2.

To compare the formulation of the model, the following initial and boundary conditions are defined regarding the reactor configuration and operating procedure described earlier.

Initial Conditions:

At $t = 0$

$$\xi = 1.0,\ \frac{\theta}{\theta_o} = 1.0,\ \frac{a}{a_o} = 1.0,\ \theta_o = \theta_{dsco} \text{ within substrates,}$$

$$\text{and } \theta_o = 1.0 \text{ elsewhere.} \tag{12}$$

Boundary Conditions:

Reactor Inlet ($z = 0.0$):

From $r = 0$ to R_{in} (gas flow inlet)

$$\omega_1 = \omega_{1o}, \quad \omega_2 = \omega_{2o}, \quad T = T_{in},$$

$$\text{and } Q = \text{vol. feed rate (STP)}. \tag{13}$$

From $r = R_{in}$ to $R_{r\times r}$ (solid wall at inlet)

$$v_r = 0.0, \quad v_z = 0.0, \quad T = T_{wall}(z = 0)$$

$$\text{and } r_d = \frac{k_d'}{a_o}\omega_2 \quad \text{(wall deposition)}. \tag{14}$$

Reactor Outlet ($z = L$):

From $r = 0$ to R_{out} (gas flow outlet) $P = P_o$.

From $r = R_{out}$ to $R_{r\times r}$ (solid wall at outlet)

$$v_r = 0.0, \quad v_z = 0.0, \quad T = T_{wall}(z = L),$$

$$\text{and } r_d = \frac{k_d'}{a_o}\omega_2 \quad \text{(wall deposition)}. \tag{15}$$

Outer Reactor Wall ($r = R_{r\times r}$)

From $z = 0$ to L

$$v_z = 0.0, \quad v_r = 0.0, \quad T_{wall} = T_{wi} + Bz + Cz^2,$$

$$\text{and } r_d = \frac{k_d'}{a_o}\omega_2. \tag{16}$$

Within substrates ($r = R_i$ to R_o and $z_j = z_j$ to $z_j + L_{dsc}$)

$$v_r = 0.0, \quad \text{and} \quad v_z = 0.0. \tag{17}$$

Where θ is the substrate porosity, v_r and v_z are the radial and axial components of the velocity vector, and r_d is the rate of carbon deposition on the reactor walls per unit surface area.

Equations 1 to 7, subject to the conditions in Eqs. 12 to 17, comprise the governing equations for the CVI reactor model and represent the processes considered important in densification of porous materials by CVI. The solution of this set of coupled nonlinear equations was accomplished numerically using the computational fluid dynamics software, PHOENICS (1987a,b, 1989) developed by CHAM.

The PHOENICS computational fluid dynamics software was utilized to solve the transport equations for momentum, heat and mass transfer to obtain the values of v_r, v_z, T, P, ω_1, ω_2, and ξ at each point in the solution domain. A uniform solution grid was defined for the reactor with 50 grid points in the radial direction and 400 in the axial direction. This grid provided acceptable resolution of the flow field around the stack of substrates and the concentration and porosity profiles within the substrates. To obtain the gas density, the infiltration gas mixture was considered to be an ideal gas, and because the feed was diluted in an inert carrier gas, changes in the molar flow rate were neglected. Since axial temperature profiles measured in a laboratory CVI reactor showed negligible heat of reaction effects during feeding of propylene diluted in helium, heat generation due to reaction was neglected. Consequently, the momentum and heat-transfer equations (Eqs. 2 and 3) were decoupled from those for mass transport (Eq. 4) and the pore radius (Eq. 7). Thus, the velocity and temperature fields were calculated only at the initial time and held constant throughout each simulation. The velocity, pressure, temperature and initial ω_1 and ω_2 fields were determined throughout the reactor at the initial conditions, Eq. 12, and then the solver stepped through time solving for ω_1, ω_2, and ξ at each step. Multiple solution sweeps through the domain were required at each time step to converge upon a solution. Upon determination of ξ, the porosity profiles in the substrates were calculated according to the random pore model (Table 2), and subsequently, the mass gain of each substrate was obtained by the following integration.

$$M = \rho_c V_{sub}\theta_o - \rho_c \int_{V_{sub}} \theta\, dV \tag{19}$$

Where, M is the mass of carbon deposited and V_{sub} is the substrate volume. The above integral was evaluated numerically for each substrate in the reactor using the calculated porosity values.

Application of model to carbon infiltration from propylene

In order to examine the behavior of a realistic CVI system, simulations were conducted for the CVI of carbon from propylene diluted in helium at atmosphere pressure. This system was well characterized by the investigations and results published previously (McAllister and Wolf, 1991; McAllister et al., 1990) giving values for the necessary kinetic parameters, substrate properties, and mass transport properties. The reactor configuration shown in Figure 1 is an accurate representation of a multisubstrate pilot-scale CVI reactor utilized industrially for intermediate studies between a bench reactor and full-scale production. A set of dimensions for this reactor and the uninfiltrated carbon composite substrates used in the simulations which follow are given in Table 3. The structural properties of the composite substrates were the same as the carbon composite materials described previously (McAllister et al., 1990) and are given in Table 4 along with the required thermal properties. The kinetic parameters determined previously (McAllister and Wolf, 1991; McAllister et al., 1990) for propylene pyrolysis and carbon deposition are listed in

Table 3. Reactor and Substrate Dimensions for CVI Model

Dimensions	Symbol	Value
Reactor Dimensions		
Length	$L_{r\times r}$	0.610 m
Radius	$R_{r\times r}$	0.0699 m
Inlet Radius	R_{in}	0.02 m
Outlet Radius	R_{out}	0.02 m
Preheat Length	L_{pre}	0.127 m
Substrate Dimensions		
Inner Radius	R_i	0.0270 m
Outer Radius	R_o	0.0508 m
Thickness	L_{dsc}	0.0127 m

Table 4. Carbon Composite Substrate Properties

Substrate Property	Symbol	Value
Initial Porosity*	θ_o	0.25
Initial Pore Radius*	r_{po}	1.15×10^{-6} m
Surface Area/Volume*	a_o	8.9×10^{5} m^{-1}
Thermal Conductivity**		
$\perp$ to fibers	$k_\perp$	8-9 (W/m·K)
$\parallel$ to fibers	$k_\parallel$	35-40 (W/m·K)

*Experimentally measured (Eq. 17).
**Private communications.

Table 5. In addition, several constants and transport properties are required, and these are listed in Table 6.

With the quantities specified in Tables 3 to 6, the parameters used in the CVI reactor model were determined experimentally, either from prior modeling studies or from the literature, or estimated using accepted correlations. Thus, the model contained no adjustable parameters, therefore the operating conditions were varied to evaluate the performance of the CVI reactor under a range of different temperatures, feed rates, propylene feed concentrations, and intersubstrate spacings. Although simulations can be calculated for widely varied sets of operating conditions, the constraints imposed by the range of conditions over which the kinetic parameters were determined present practical limits for conditions of reactor simulations. The kinetic parameters for propylene pyrolysis and carbon deposition were determined from experimental data obtained at temperatures from 675-810°C and C_3H_6 feed concentrations from 5 to 15%. Outside these ranges and particularly at temperatures above 810°C, significant changes in the kinetics of carbon deposition from propylene were observed. Therefore, the simulations reported here were limited to operating conditions within the range of confidence of the kinetic parameters.

Results and Discussion

To characterize the behavior and performance of the CVI reactor configuration presented earlier, simulations were run at various volumetric feed rates, propylene feed concentrations and the reactor wall temperatures. In addition, the effects of variations in the spacing between substrates were determined by simulation. Because of the large number of dependent variables and the transient nature of the simulations, the parametric survey provided much more information than is practical to present here. Thus, results are displayed and discussed in detail for only one simulation conducted at moderate infiltration conditions. The time dependent behavior of the CVI reactor is highlighted for this standard case. The detailed results and discussion of the standard case should provide a basic understanding of the primary physical, chemical and transport processes occurring in the CVI reactor. The major effects of other operating conditions are summarized thereafter.

Table 5. Kinetic Parameters Required in the CVI Reactor Model

Reaction	Symbol	Value
Pyrolysis of Propylene		
Preexponential Factor	k_{1o}	10^{13} mL$^{0.45}$/mol$^{0.45}$·s
Activation Energy	E_1	57.0 kcal/mol
Carbon Precursor Formation		
Preexponential Factor	$k_{io}M_2$	15.26 kg/mol·s
Activation Energy	E_i	22.34 kcal/mol
Carbon Precursor Deposition		
Preexponential Factor	k_{do}	7.704×10^{9} m/s
Activation Energy	E_i	71.16 kcal/mol

Table 6. Properties of Helium and Propylene Required in the CVI Model

Property	Symbol and Units	Value
Helium Properties*		
Molecular Weight	M (kg/mol)	0.0040026
Viscosity	μ (N·s/m^2)	$1.41\times10^{-6}\,T^{1/2}$
Heat Capacity	C_p (J/kg·K)	5,193
Prandtl Number	Pr	0.654
Thermal Conductivity	k (W/m·k)	$-0.114+0.0148\,T^{1/2}$
Propylene Properties		
Molecular Weight	M_1 (kg/mol)	0.04208
Molecular Diffusivity in He**	D_{AB} (m^2/s)	$3.322\times10^{-4}\left[\frac{T(\mathrm{K})}{1{,}008}\right]^{1.5}$

*Properties of He taken from Incropera and Dewitt (1925).
**Estimated.

For the parametric studies, the wall temperature profile was specified by Eq. 20 which gave the following profile.

$$T_{wall} = T_{wi} + 553.8\ z - 707.7\ z^2 \tag{20}$$

The parabolic wall temperature profile of Eq. 20 was used because it approximated the wall temperature profile measured experimentally in a pilot CVI reactor to be discussed later. Using Eq. 20, the reactor wall temperature was set and shifted up or down depending on the choice of T_{wi}, which was the inlet wall temperature. The maximum wall temperature occurred at $z/L = 0.64$ and the difference between the maximum wall temperature and T_{wi} was constant at 108°C.

Time dependent CVI reactor behavior

For the standard case, the operating conditions specified were a volumetric feed rate of 40 cm^3/s at 25°C and 1 atm., a propylene feed mole fraction of 0.05, a feed temperature of 500°C, an inlet wall temperature of 650°C and the spacing between substrates was 1.0 cm. The results of this simulation are shown in Figures 2 to 6 in the form of the mass of carbon deposited, velocity vectors, and contour plots of the temperature, substrate porosities and the carbon precursor concentration field. For the reasons discussed above, the temperature, pressure and velocity fields were solved at steady state and held constant for the entire simulation. The temperature field determined for these variables under the conditions of this simulation is shown in Figure 2. The temperature was lowest at the inlet because the feed gases were cooler than the lowest wall temperature. In the preheat zone, the internal temperature profiles became relatively flat and radial temperature gradients were minor. The temperature increased to the specified maximum of 760°C at $z/L = 0.64$ and then decreased towards the outlet. The calculated velocity vectors are shown in Figure 3, and for the standard case simulation, the highest axial velocities occurred at the inlet and outlet due to the decreased entrance

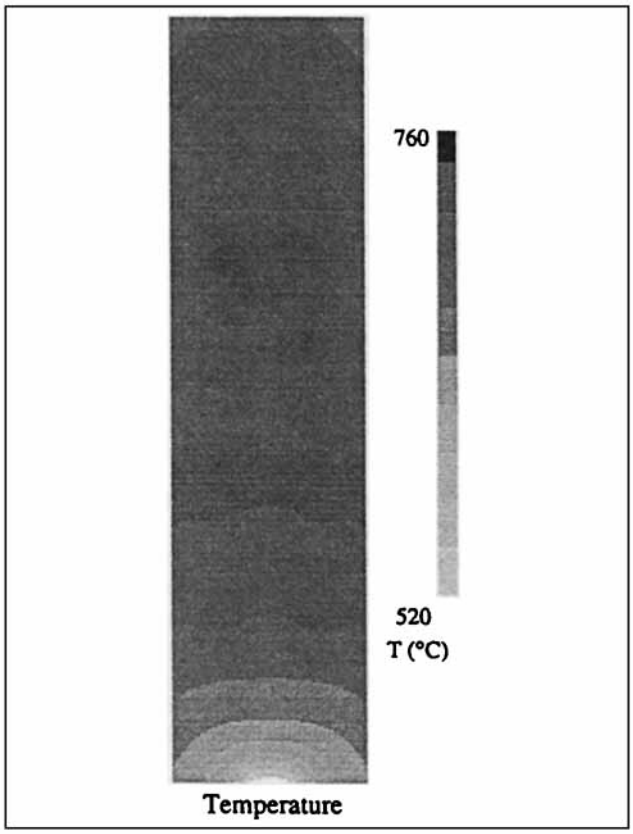

Figure 2. Steady-state temperature fields for the standard case CVI reactor simulation.

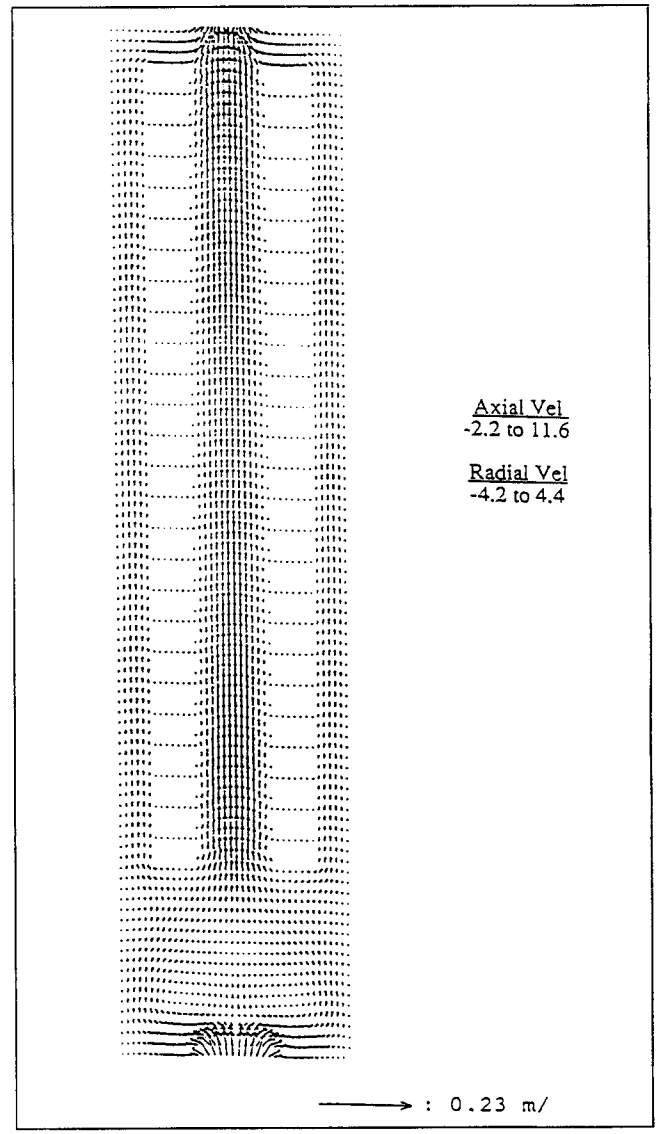

Figure 3. Steady-state velocity vectors for the standard case CVI reactor s.

and exit radii. Within the reactor, the highest positive axial velocity occurred in the center of the reactor, while slower flow occurred outside the stack of substrates. Almost no radial or axial flow occurred between the discs, and according to Eq. 17, the velocity was zero within the porous substrates. The radial velocity component was most significant near the inlet and the outlet under these conditions.

In Figure 4, the mass of carbon deposited in each substrate normalized by the maximum mass gain is displayed as a function of dimensionless position in the reactor with zero corresponding to the inlet at the bottom of the reactor and 1.0 to the outlet at the top of the reactor. Results are shown at intervals of 50 h for the first 200 h of infiltration and at 100 h intervals from 200 to 400 h. The mass deposited in each substrate increased with time until a maximum level of densification was approached at 400 h. Under the conditions of this simulation, and primarily due to the imposed temperature profile, the middle substrates were infiltrated at a higher initial rate, which led to a maximum mass gain at z/L approximately equals 0.5 after 100 h. The mass deposited increased more slowly at the bottom and the top of the stack of substrates. However after 400 h, the mass of carbon deposited within the top and bottom substrates became greater than in the middle of the stack. The temperature was lowest at the bottom of the reactor, thus deposition was slowest in the lower substrates, but because of the lower deposition rate, more uniform infiltration occurred and the mass of carbon deposited was higher.

In Figure 5, magnified views of selected substrates from the bottom, middle and top of the reactor are shown to provide a clearer image of the variation in porosity with time at different locations in the reactor. After 50 h of infiltration, the porosity of the substrate from the center of the reactor had decreased to the greatest extent especially around the edges, but relatively little deposition had occurred in the top and bottom substrates. As time increased to 100 and 200 h, pore closure at the outer surface of the center substrate occurred first and the residual internal porosity was highest for this substrate. The substrate located near the top of the reactor was densified to a slightly higher level than the middle substrate with the residual internal porosity in the range of 0.6 to 0.7. The normalized porosity of the substrate at the bottom of the reactor, which was at the lowest temperature, was infiltrated more slowly, but the residual internal porosity after 400 h was significantly lower than for the other substrates.

The CVI reactor model also accounted for the mass transport of propylene and the carbon precursor within the reactor and

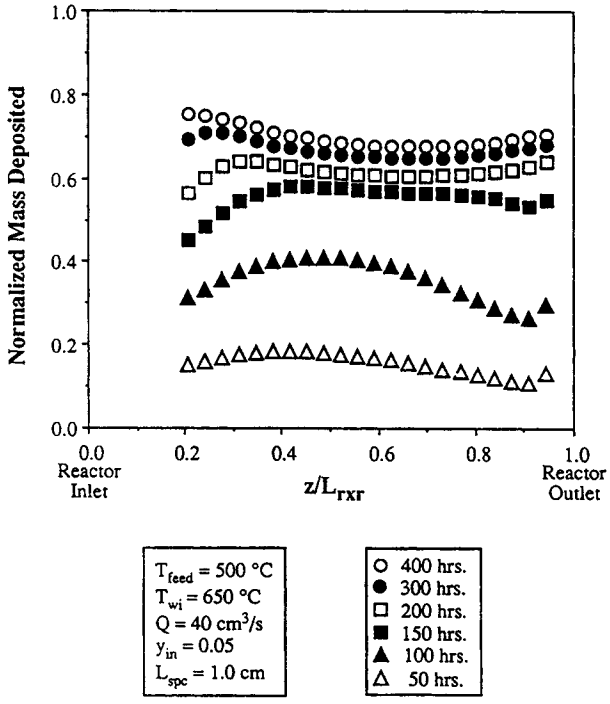

Figure 4. Normalized mass gain of each substrate vs. axial position at several times in the infiltration process for the standard set of conditions.

the porous substrates. The propylene concentration profiles did not vary significantly with time except within the substrates. For these conditions, the C_3H_6 concentration within the substrates was lowered markedly only when the porosity was near zero. Since the rate of deposition was directly related to the carbon precursor concentration, it was important to examine the precursor concentration contours and the changes which occurred over time. Precursor concentrations at the initial time, and after 50, 100, 150 and 200 h are shown for the entire reactor in Figure 6. At the initial time, a maximum concentration occurred at the top of the preheat zone. As time proceeded, the maximum increased in magnitude and shifted towards the top of the reactor. In the early stages of infiltration, most of the precursor was depleted by deposition before reaching the top of the reactor. However, as substrates became filled with carbon, the amount of accessible surface area for deposition decreased due to closing of the internal pore structure, which increased diffusional limitations and resulted in increased bulk precursor concentrations. After 200 h, the precursor concentration contours did not change except near the bottom substrates, where the pores were not blocked completely by deposition.

Effects of temperature on CVI

Since temperature was shown to have important effects on propylene pyrolysis and carbon deposition rates (McAllister et al., 1990), CVI processes at different temperatures were simulated. To investigate the effects of different reactor temperatures on CVI reactor performance, three temperature profiles of the same form but differing magnitudes were specified at the outside wall of the cylindrical reactor by changing the wall temperature at the reactor inlet. In the three cases simulated, the wall temperature at the inlet was set at 625, 650 and 700°C, respectively, and the magnitude of the maximum temperature was equal to 733, 758 and 808°C. After 50 h of infiltration as shown in Figure 7a, at the highest inlet temperature of 700°C, the greatest amount of deposition occurred

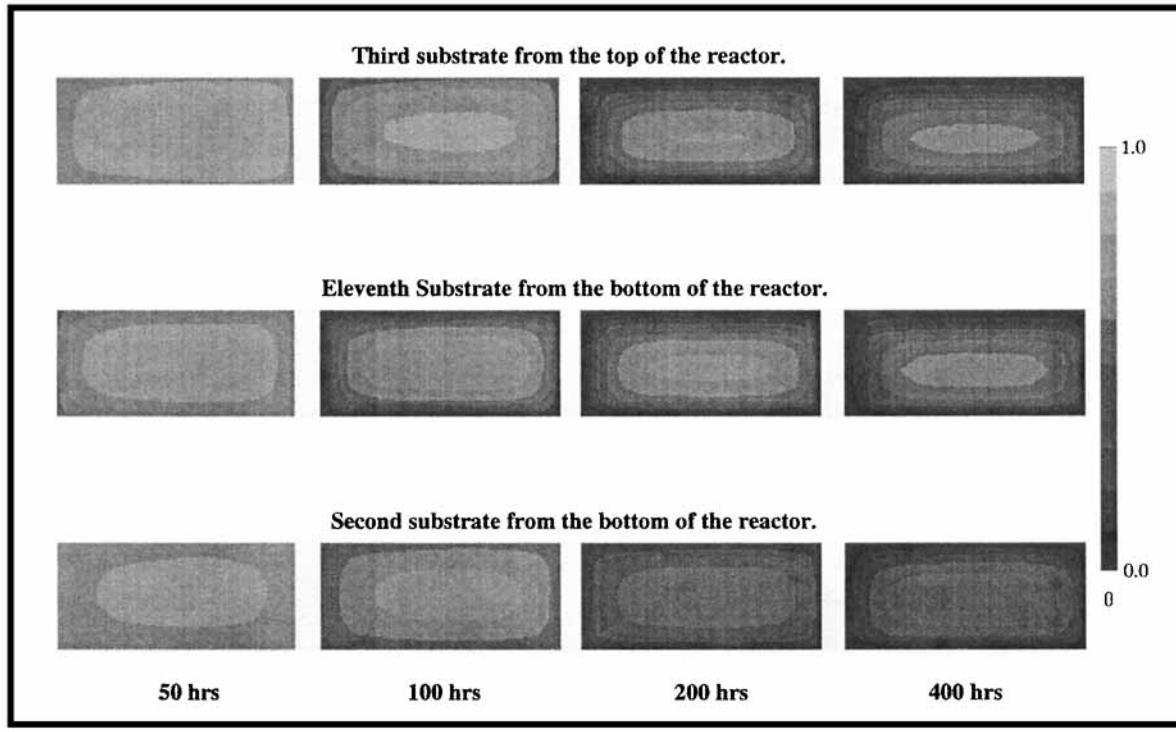

Figure 5. Porosity contours of selected substrates at 50, 100, 200, and 400 h of CVI at the standard conditions.

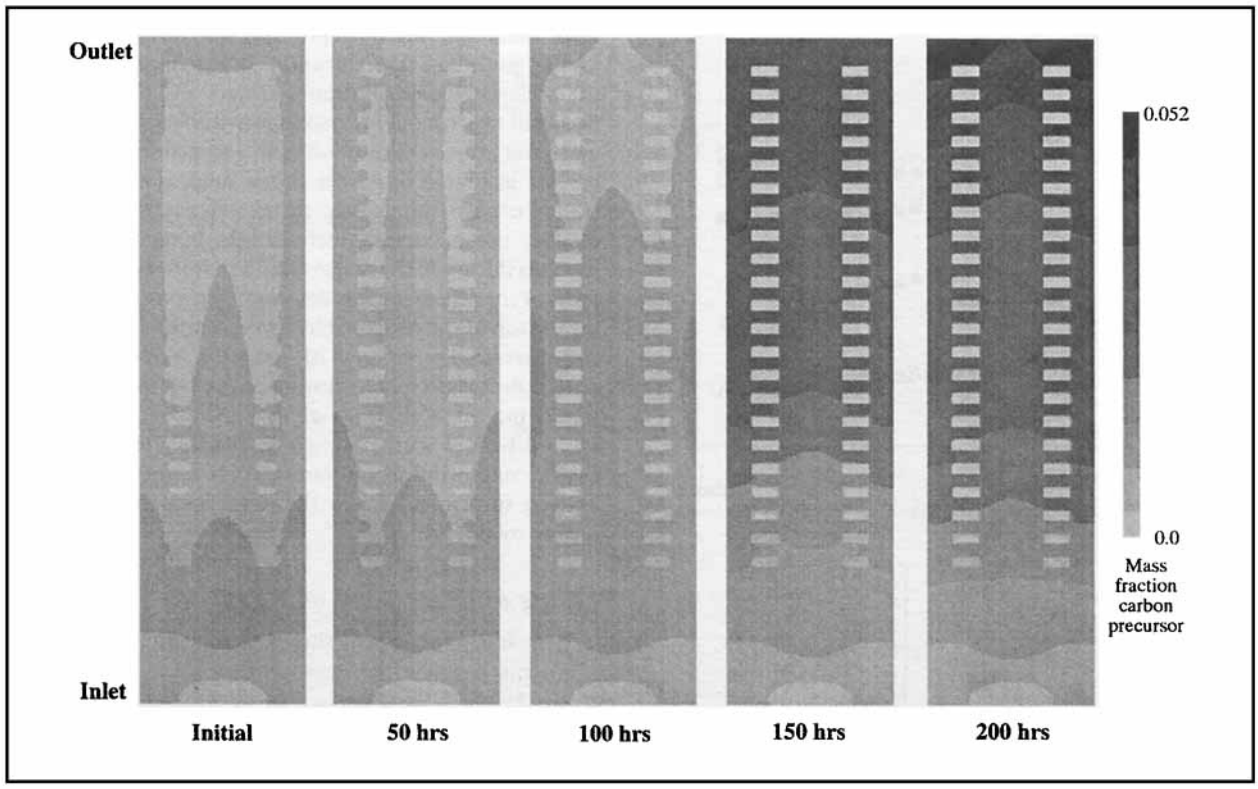

Figure 6. Carbon precursor concentration contours at 0, 50, 100, 150 and 200 h of CVI at the standard conditions.

at the bottom of the stack of substrates and declined to smaller values at the top of the reactor. At the intermediate temperature (650°C), the mass deposited within the lower substrates was reduced, and a maximum in mass gain occurred at $z/L = 0.45$. At the lowest inlet temperature, infiltration was slower in all of the substrates except in the top seven discs where the mass deposited was higher than for the high wall temperature, but slightly lower than at the intermediate temperature. After 100 h as shown in Figure 7b, the mass gain at the highest temperature did not increase significantly over that at 50 h in the lower half of the reactor, but the substrates in the top half of the reactor were densified to levels comparable to the lower substrates. At the intermediate wall temperature, densification was similar in almost all of the substrates, however, the bottom substrates were not as densified, yet. At the lowest inlet temperature (625°C), a large difference was apparent between the most infiltrated substrate and the least densified.

From the final mass gain results shown in Figure 7c, it was apparent that the reactor temperature had a major impact on both the mass of carbon deposited within the substrates and

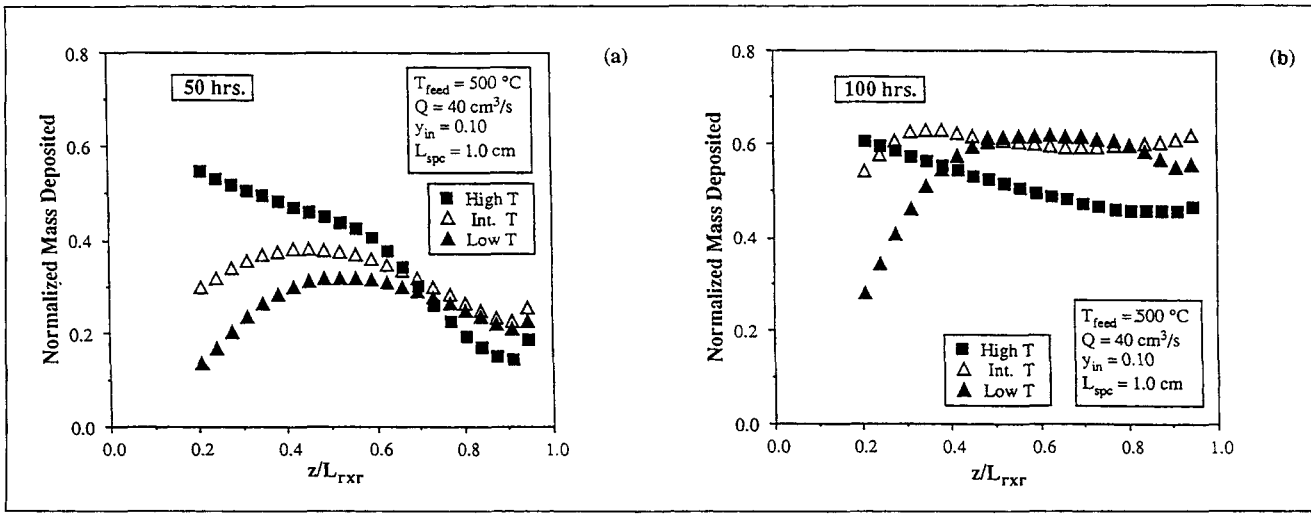

Figure 7. The normalized mass gain of each substrate vs. axial position in the reactor for low, intermediate and high reactor temperatures: (a) at 50 h; (b) at 100 h; (c) at the final time for each temperature.

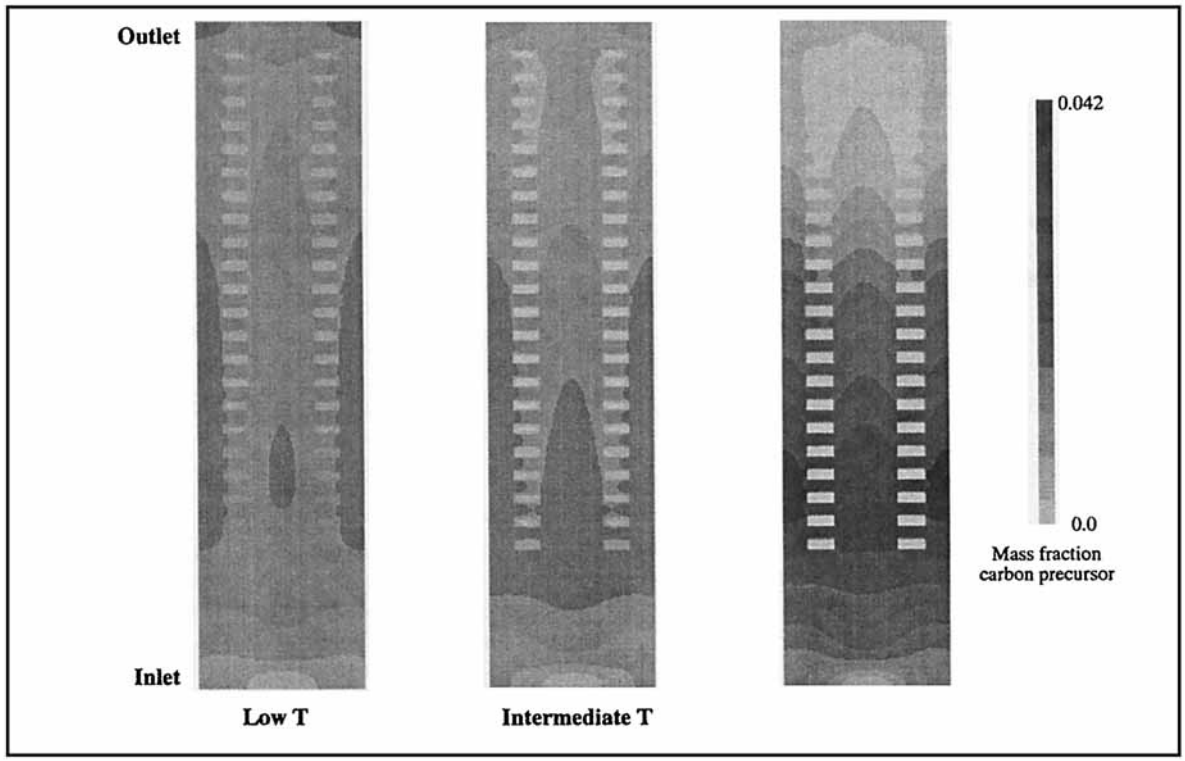

Figure 8. Carbon precursor concentration contours after 50 h of CVI for three different wall temperature profiles.

the time required to achieve the final level of infiltration. The lowest wall temperature gave the highest level of infiltration as the mass gain approached 90% of the maximum gain, however at the expense of longer times. At the intermediate temperature, the normalized mass deposited decreased to approximately 0.75, but the time decreased by a factor of two from 400 to 200 h. At the high temperature, the time required to reach the final level of infiltration was only 100 h, however, the normalized mass deposited was significantly lower and varied from 0.62 at the highest densified substrate to <0.5 near the top of the reactor. Because the rate of deposition increased relative to the rate of diffusion within the substrates at higher temperatures, densification became more nonuniform and the final mass gain decreased with temperature, however the time for pore closure decreased as well.

The simulated results, which best explained the temperature behavior of the CVI reactor were the carbon precursor concentration contours along the reactor. The contours after 50 h are displayed in Figure 8 and in all three simulations, a maximum precursor concentration occurred near the bottom of the substrate stack. The location shifted towards the top of the reactor as the wall temperature decreased, because less precursor formed in the preheat zone and the rate of deposition was relatively low at the temperature of the bottom substrates. Conversely, at the highest temperature, the precursor was depleted rapidly by deposition and very low concentrations of the precursor existed in the top half of the reactor. These observations explained the mass gain behavior for the different temperatures shown in Figure 7a. At the high temperature, high infiltration rates within the lower substrates depleted the precursor. Thus, in the middle and near the top of the reactor, even though the reactor temperature was high, the amount of precursor present was low and the rate of deposition was limited.

Effects of flow rate on CVI

The feed rate to the CVI reactor was identified as another operating condition which could be varied and thus simulations at various flow rates were conducted. For the reactor under consideration, the volumetric feed rate at 25°C and atmospheric pressure was varied from 20 to 60 cm^3/s, which corresponded to gas phase residence times in a loaded reactor at the maximum wall temperature of 37 to 112 s. The influence of the flow rate on the mass of carbon deposited within the substrates along the length of the reactor was most significant at intermediate times, as shown in Figure 9 at 100 h. For the low flow simulation, after 100 h the normalized mass gain was highest for the bottom substrate and decreased towards the top substrate. As the flow rate increased, the maximum infiltration rate shifted up the reactor as less of the carbon precursor formed in the preheat zone. Thus, at higher flow rates, the mass deposited in the top substrates increased. At low flow rates, the precursor was depleted from the gas phase before reaching the top of the reactor resulting in higher mass gains of the lower substrates at short process times. Although densification depended on flow rate at intermediate infiltration times, the final level was independent of flow rate.

Effects of propylene feed concentration on CVI

The third main operating variable in the CVI of porous substrates with carbon is the concentration of the parent hy-

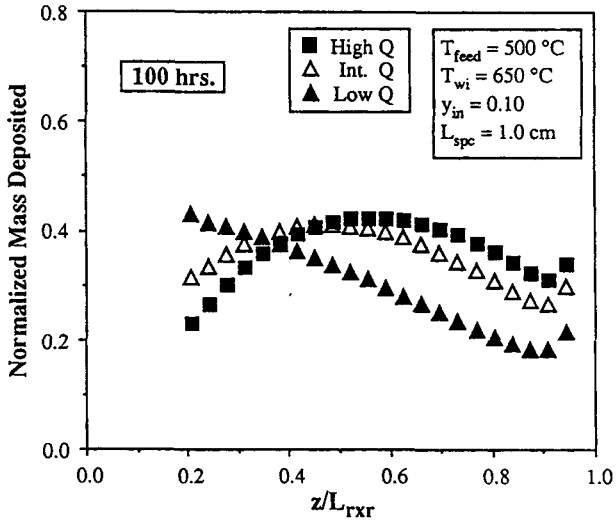

Figure 9. Normalized mass gain of each substrate vs. axial position in the reactor for low, intermediate and high volumetric flow rates at 100 h.

drocarbon in the reactor feed. The parent hydrocarbon was the source of carbon in the simulations and thus, it was important to investigate the effects of changes in the hydrocarbon feed concentration on substrate densification. Simulations at propylene feed mole fractions of 0.05, 0.10 and 0.15 showed that the final mass of carbon deposited in the individual substrates was independent of the C_3H_6 concentration, however, the time required to reach the final level was reduced significantly at higher feed fractions. At higher propylene feed concentrations, the supply of carbon to the reactor became less of a factor in limiting deposition throughout the reactor. Thus, all the substrates were densified more rapidly, however, the fraction of the carbon in the feed converted to the desired product decreased as the feed fraction increased.

Effects of the substrate separation

Another variable which warranted study was the distance between individual substrates in the CVI reactor. Thus, simulations were conducted for varied separations to determine the effects of disc spacing on CVI. The substrate spacings examined were 0.5, 1.0 and 2.0 cm with the number of substrates loaded in the reactor equal to 28, 22 and 15, respectively. Under these conditions, the final mass deposited in all of the substrates after 400 h was comparable for all three spacings and the time required to reach this level was only slightly longer for the smaller spacings. According to these simulations, the smallest disc spacing provided densification of more substrates at approximately the same final time. Thus, the smallest gap between substrates, which does not severely limit access of the gas phase to the stagnant regions between discs is the optimum choice.

Comparison of CVI Reactor Simulations with Experimental Data

Conditions of experimental results

In order to determine the quantitative predictive capabilities of the CVI reactor model, model predictions were compared with experimental results obtained in a pilot-scale reactor. Experimental results have been obtained for chemical vapor infiltration of carbon fiber/resin char matrix substrates from propylene in the CVI reactor shown in Figure 1 and model predictions are compared to these results in this section. The pilot-scale reactor results were obtained elsewhere in an industrial research laboratory. The experimental conditions were somewhat different from the conditions of the previous simulations so that some minor modifications were made to the model. First of all, nitrogen was used as the carrier gas, which required adjustment of several gas phase properties. The new parameters used with N_2 as inert diluent are shown in Table 7.

Table 7. Properties of Nitrogen Required in the CVI Model

Property	Symbol and Units	Value
Nitrogen Properties*		
Molecular Weight	M (kg/mol)	0.028013
Viscosity	μ (N·s/m^2)	$1.52\times10^{-6}\,T^{1/2}$
Heat Capacity	C_p (J/kg·K)	5,193
Prandtl Number	Pr	0.654
Thermal Conductivity	k (W/m·K)	$-0.042+3.39\times10^{-3}\,T^{1/2}$
Mol. Diff. of C_3H_6 in N_2	D_{AB} (m^2/s)	$3.322\times10^{-4}\left[\frac{T(K)}{1{,}008}\right]^{1.5}$

* Properties of N_2 taken from Incropera and Dewitt (1985).

To determine the wall temperature profile for the pilot CVI reactor, a thermocouple was placed between the graphite susceptor and the outer reactor casing, as shown in Figure 1. A piecewise linear fit to the temperature profile was made which yielded the following equations for the wall temperature in the CVI reactor model.

$$T_{wall} = 583 + 2{,}179\,z \quad \text{for} \quad z = 0 \text{ to } 0.076 \text{ m} \tag{21}$$

$$T_{wall} = 734 + 154.1\,z \quad \text{for} \quad z = 0.076 \text{ to } 0.279 \text{ m} \tag{22}$$

$$T_{wall} = 828 - 160.8\,z \quad \text{for} \quad z = 0.279 \text{ to } 0.483 \text{ m} \tag{23}$$

$$T_{wall} = 939 - 393.7\,z \quad \text{for} \quad z = 0.483 \text{ to } 0.6096 \text{ m} \tag{24}$$

The maximum wall temperature was 780°C, the wall temperature at the inlet was 590°C and the gas inlet temperature was 500°C. Within the load zone of the reactor, 20 substrates were placed which had the same dimensions as given in Table 3 and with the spacing between substrates being 0.635 cm. The volumetric feed rate to the reactor was 85.3 cm^3/s (STP), which translated to a gas phase residence time at the maximum reactor temperature of 26.1 s. The mole fraction of C_3H_6 in the feed was 0.05. All other reactor dimensions and parameters were as defined previously, and the kinetic expressions determined in a helium carrier gas were assumed to apply with N_2 as a carrier gas as well. As stated earlier, all model parameters were determined experimentally, via prior modeling studies, from the literature or using accepted correlations so that there were no adjustable parameters.

Comparison of experimental results and simulations

Experimental results obtained under the conditions de-

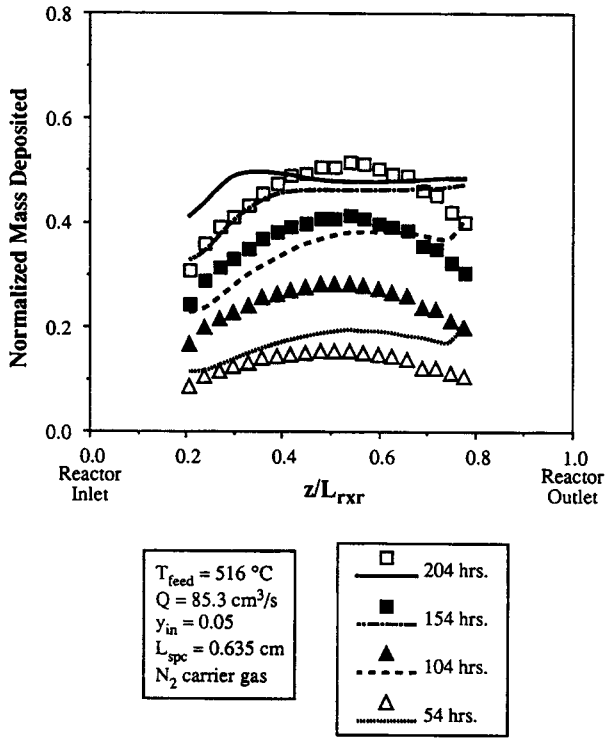

Figure 10. Comparison of CVI reactor model simulation results with experimental results for infiltration of carbon fiber substrates with carbon from propylene.

scribed earlier were obtained, and a CVI reactor simulation was run for this set of conditions. The experimental results were provided in terms of the mass of each substrate after 54, 104, 154 and 204 h of densification and were obtained by stopping the reactor operation at the desired time and unloading and weighing each disc. After each intermediate time, the discs were reloaded into the reactor in the same position as previously and the reactor was restarted under the same operating conditions. For purposes of comparison, theoretical predictions were calculated via the CVI reactor model at each of these times.

The experimental and theoretical results are compared in Figure 10 with the experimental data represented by symbols and the model predictions presented as lines. It should be reiterated that no adjustable parameters were used to fit the model predictions to the experimental results. The reactor operating conditions were the only input to the model. At 54 h of infiltration, the agreement between theory and experiment was good for the lower substrates, but the predictions for mass gain were higher than the experimental data in the upper portion of the reactor. Also, the high mass gain predicted for the top substrate was not observed experimentally. At 104 h, the theoretical values are well above the experimental data resulting in poor agreement. According to the model, the substrates in the upper half of the reactor should have been densified at nearly the same rate; however, the experimental results showed that the middle substrates were densified at the highest rate while the mass gains of the substrates at the top and bottom of the reactor lagged in densification. As time proceeded to 154 h, the experimental rate of infiltration had not slowed significantly and the highest mass gain was still in the center of the reactor. At 154 h, the rate of increase of the mass gains predicted by the simulation had slowed so that the change in the mass gain of the substrates from 104 to 154 h was reduced from the previous 50 h. After 204 h, the increase of the experimental mass gain had slowed but not drastically as predicted by the simulation, however, the simulated results showed significant mass gains only in the bottom substrates while densification had slowed drastically in the rest of the reactor.

Overall, the best agreement between theory and experiment occurred for the bottom substrates. In the remainder of the reactor, the model overpredicted the mass of carbon deposited for the first 154 h and then predicted too rapid a decline in the infiltration rate at later times. Several possible explanations exist which could explain the discrepancies between the CVI simulation and experimental results. First, the temperature at which the experimental results were obtained may have been too high. Satisfactory agreement between theory and experiment in the single substrate CVI model (McAllister and Wolf, 1991) was limited to temperatures below 765°C. Thus, the extrapolation of the kinetic parameters determined in the model calibration to higher temperatures may not be valid. Also, since the kinetic parameters and transport properties obtained from the literature (McAllister and Wolf, 1991; McAllister et al., 1990) were determined from data obtained with He as the carrier gas, the switch to N_2 may have caused some unforeseen changes in reaction kinetics and/or gas phase transport. Because pyrolytic carbon deposition involves homogeneous nucleation of carbon precursors, the effects of the carrier gas could be significant especially since He is a light monatomic gas and N_2 is a heavier diatomic gas. Another explanation is that the temperature profile specified at the wall was not accurate. Although the temperature was measured at several locations along the reactor wall, the actual readings were taken between the graphite susceptor and the outer reactor wall. Thus, the temperature on the inside of the susceptor, which is the outer wall at which the temperature should be specified, may have been lower. Based on the results reported earlier, it appeared that the temperature throughout the reactor may have been too high in the simulation. Another difference between the acquisition of results in the pilot-scale reactor was the requirement to stop the operation and weigh the substrates. This exposure to air might have altered the properties of the substrate surface leading to higher carbon deposition than predicted by the laboratory scale results.

The fact that the model predicted a more rapid decline in the mass deposited was not surprising in light of the data and model predictions presented by McAllister and Wolf (McAllister and Wolf, 1991) which showed that at high temperatures, the single substrate model predicted a more rapid decrease in the rate of deposition than occurred experimentally. This difference was attributed mainly to outer surface deposition which was not accounted for in the single substrate model. Outer surface deposition was not included in this model either and could have caused some of the discrepancies shown in Figure 10. Another possible explanation concerns the substrates used by McAllister and Wolf (1991) in the long run CVI experiments and the larger materials used in this work. The substrates for the laboratory reactor were cut and machined from substrates of the same structure as those used here, but due to the composite nature of these materials, different fiber alignments were present in different parts of these

substrates. Thus, the properties of the small substrates may not have been the same as the average properties of the larger samples. Probably, a combination of these factors resulted in the differences between theory and experiment, and more experimental investigations and model refinements are required to determine the primary causes and to improve quantitatively the predictive capabilities of the model. Overall, the final mass gain predicted by the model is within 15% of the experimentally observed values for most of the substrates. Considering that a reactor simulation may be run in a few hours as compared to the two week period required to obtain the data shown in Figure 7, the results are rather satisfactory, especially considering the complexity of the chemistry, fluid flow and transport phenomena involved.

Conclusions

The CVI reactor simulations conducted indicate the following effects of operating conditions on reactor performance:

(*a*) The reactor temperature has the most significant impact of all the variables examined. As the temperature increases, the rate of deposition increases, the time over which significant densification occurs decreases and the carbon yield increases, but higher temperatures also increase the nonuniformity of densification resulting in lower mass gains.

(*b*) The volumetric feed rate to the reactor affects the manner in which substrates are densified along the length of the reactor. At low flow rates, the substrates nearest the inlet of the reactor are densified first and densification proceeds gradually down the length of the reactor as less of the precursor is depleted in the bottom of the reactor. At higher flow rates, higher precursor concentrations occur towards the top of the reactor so that densification proceeds more rapidly in the center of the reactor. The final level of densification and the time required to reach this level are relatively independent of flow rate, but the carbon utilization decreases significantly as the flow rate increases.

(*c*) As the propylene feed concentration increases, the level of densification at intermediate times throughout the reactor increases as well. At high propylene concentration, the depletion of carbon precursor from the bulk stream is less significant enabling infiltration to proceed throughout the reactor. Even though densification occurs more rapidly at higher C_3H_6 concentrations, the final level of densification is relatively independent of the concentration.

(*d*) As the spacing between substrates increases, the rate of densification increases throughout the reactor, because there are fewer substrates and consequently less surface area for deposition and higher precursor concentrations. The final level of densification is not dependent on the spacing, but more substrates are densified in only slightly longer times at smaller spacings.

Comparison between experimental pilot reactor results and model predictions were satisfactory at short times and long times, but agreement was less satisfactory at intermediate times. More investigations, including laboratory-scale and pilot-scale studies and model refinements, are required to improve quantitative agreement between the CVI model and pilot plant results.

The results presented in this study provide valuable insights into the CVI process and the effects of various operating conditions on reactor behavior. The knowledge acquired can be used to guide the engineer in the selection of the optimal reactor operating conditions. For instance, the reactor temperature has a major impact on the uniformity of densification and the time over which infiltration occurs, thus the operating temperature must be selected such that the desired substrate density is achieved in the shortest amount of time. Also, the parent hydrocarbon feed concentration and the feed flow rate can affect the reactor performance. Of course, economic factors including utility and feed gas costs in conjunction with final product specifications will dictate the optimum set of operating conditions, and a CVI reactor model of this type which is based on fundamental transport processes is a valuable tool in evaluating various sets of operating conditions.

Notation

a = surface area per unit volume
C_p = heat capacity
D_{eff} = effective mass diffusivity
g = gravitational force vector
k = thermal conductivity
k_1' = rate constant for conversion of propylene
k_i' = rate constant for formation of carbon precursor
k_d' = rate constant for deposition of carbon precursor
k_r' = rate constant for change of pore radius
L_{dsc} = substrate thickness
L_{pre} = length of reactor preheat zone
$L_{r\times r}$ = reactor length
L_{spc} = spacing between substrates
M_1 = molecular weight of propylene
P = pressure
Q = volumetric flow rate
r_{po} = initial pore radius
R_i = inner substrate radius
R_{in} = reactor inlet radius
R_o = outer substrate radius
R_{out} = reactor outlet radius
$R_{r\times r}$ = reactor radius
t = time
T = temperature
T_{in} = wall temperature at the reactor inlet
v = velocity vector
v_r = radial velocity component
v_z = axial velocity component
V_{sub} = substrate volume
y_{in} = hydrocarbon feed mole fraction

Greek letters

θ = substrate porosity
μ = viscosity
ξ = dimensionless pore radius normalized by the initial pore radius
ρ = gas phase density
ρ_c = density of deposited carbon
τ = stress tensor
ω = mass fraction

Literature Cited

Bird, R. B., W. E. Stewart, and E. N. Lightfoot, *Transport Phenomena*, John Wiley & Sons, New York, p. 511 (1960).

Chung, G. Y., B. J. McCoy, J. M. Smith, D. E. Cagliostro, and M. Carswell, "Chemical Vapor Infiltration: Modelling Solid Matrix Deposition in Ceramic-Ceramic Composites," *Chem. Eng. Sci.*, **46**(3), 723 (1991).

Chung, G. Y., and B. J. McCoy, "Modeling of Chemical Vapor Infiltration for Ceramic Composites Reinforced with Layered, Woven Fabrics," *J. Am. Ceram. Soc.*, **74**(4), 746 (1991).

Gupte, S. M., and J. A. Tsamopoulos, "Densification of Porous

Materials by Chemical Vapor Infiltration," *J. Electrochem. Soc.*, **136**(2), 555 (1989).
Gupte, S. M., and J. A. Tsamopoulos, "An Effective Medium Approach for Modeling Chemical Vapor Infiltration of Porous Ceramic Materials," *J. Electrochem. Soc.*, **137**(5), 1626 (1990).
Guzman, G. L., and E. E. Wolf, "Effect of Nonuniform Activity Distribution on Catalyzed Gas-Solid Reactions," *Ind. Eng. Chem. Fundam.*, **18**(1), 7 (1979).
Houtman, C., H. Moffat, and K. F. Jensen, "Large Scale Finite Element Computations of Reacting Flows in CVD Reactors," *Fifth European Conference on CVD*, Uppsala, Sweden (1985).
Incropera, F. P., and D. P. Dewitt, *Fundamentals of Heat and Mass Transfer*, 2nd ed., John Wiley & Sons, New York (1985).
Jensen, K. F., "Modeling of Chemical Vapor Deposition Reactors," *Proceedings of Ninth International Conference on CVD*, Electrochemical Society, Pennington, NJ, p. 3 (1984).
Jensen, K. F., and D. B. Graves, "Modeling and Analysis of Low Pressure CVD Reactors," *J. Electrochem. Soc.*, **130**(9), 1950 (1983).
Jensen, K. F., and R. R. Melkote, "Chemical Vapor Infiltration of Short-Fiber Preforms," *Ext. Abs. AIChE 1989 Annual Meeting*, San Francisco, p. 541 (1989).
Kuiper, A. E. T., C. J. H. van den Brekel, J. de Groot, and G. W. Veltkamp, "Modeling of Low Pressure CVD Processes," *J. Electrochem. Soc.*, **129**(10), 2288 (1982).
Ludwig, J. C., H. Q. Qin, and D. B. Spalding, *TR/200: The PHOENICS Reference Manual*, CHAM Ltd., London (1987).
McAllister, P., and E. E. Wolf, "Modeling of Chemical Vapor Infiltration of Carbon in Porous Carbon Substrates," *Carbon*, **29**, 387 (1991).
McAllister, P., J. F. Hendricks, and E. E. Wolf, "The Infiltration of Carbon Fiber Felts and Composites by Pyrolytic Carbon Deposition from Propylene," *Carbon*, **28**, 579 (1990).
Middleman, S., "The Interaction of Chemical Kinetics and Diffusion in the Dynamics of Chemical Vapor Infiltration," *J. Mater. Res.*, **4**(6), 1515 (1989).
Middleman, S., and A. Yeckel, "A Model of the Effects of Diffusion and Convection on the Rate and Uniformity of Deposition in a CVD Reactor," *J. Electrochem. Soc.*, **133**(9), 1951 (1986).
Patankar, S. V., *Numerical Heat Transfer and Fluid Flow*, McGraw-Hill, New York (1980).
Petersen, E. E., "Reaction of Porous Solids," *AIChE J.*, **3**(4), 443 (1957).
Roenigk, K. F., and K. F. Jensen, "Analysis of Multicomponent LPCVD Processes," *J. Electrochem. Soc.*, **132**(3), 448 (1985).
Rosten, H. I., and D. B. Spalding, *TR/99: The PHOENICS Equations*, CHAM Ltd., London (1987).
Satterfield, C. N., *Heterogeneous Catalysis in Practice*, McGraw-Hill, Inc., New York, p. 336 (1980).
Spalding, D. B., *TR/100: The PHOENICS Beginner's Guide*, CHAM Ltd., London (1989).
Tai, N.-H., and T.-W. Chou, "Analytical Modeling of Chemical Vapor Infiltration in Fabrication of Ceramic Composites," *J. Am. Ceram. Soc.*, **72**(3), 414 (1989).
Yeckel, A., S. Middleman, and A. K. Hochberg, "The Origin of Nonuniform Growth of LPCVD Films from Silane Gas Mixtures," *J. Electrochem. Soc.*, **136**(7), 2038 (1989).
Yeckel, A., and S. Middleman, "Strategies for the Control of Deposition Uniformity in CVD: The Design of a Novel Wafer Carrier," *J. Electrochem. Soc.*, **137**(1), 207 (1990).

Manuscript received Dec. 6, 1991, and revision received Nov. 16, 1992.